Simulation of the Cutting Process in Softening and Hardening Soils

Zhefei Jin,[1] James P. Hambleton[2]

[1]Department of Civil and Environmental Engineering, Northwestern University, Evanston, IL 60208; e-mail: zhefeijin2015@u.northwestern.edu

[2]Department of Civil and Environmental Engineering, Northwestern University, Evanston, IL 60208; e-mail: jphambleton@northwestern.edu

ABSTRACT

Simulation of plowing and cutting processes in soils is challenging and time-consuming due to large deformations and contact interactions. Recent studies on sand have suggested that a simplified, efficient approach based on incremental plastic analysis can capture the essential physics and features of the problem. The present study refines this technique by enhancing the kinematics and implementing a more sophisticated material law. The effects of hardening and softening, as well as dilatancy and compaction, are introduced. With the modified model, it is observed in the case of hardening (compaction) that the occurrence of multiple successive shear bands at variable locations gives the appearance of continuous shearing in the final pattern of deformation. This is markedly different from the previously predicted response in the case of softening (dilatancy), where shear bands appear at distinct locations and transition from one discrete location to the next. The computed results are compared with preliminary experimental data gathered in the Soil-Structure and Soil-Machine Interaction Laboratory (SSI-SMI Laboratory) at Northwestern University.

INTRODUCTION

The mechanical process of moving and shaping soil is widely observed in natural and man-made environments, especially for civil construction and mining. Soil cutting is a fundamental mode of deformation in these processes (Hambleton et al. 2014). The term "cutting" refers to the large, progressive displacement of soil produced by a tool or object as it is pushed or dragged across the soil surface, and specifically to the case where material accumulates in front of the tool.

The problem of soil cutting has been studied using various analytical and numerical methods. Analytical methods were developed based on earth pressure theories (e.g., McKyes 1985, Godwin et al. 2007). These methods often fail to clarify the stage of cutting and do not consider the full process of deformation. Accumulated soil is often neglected entirely, or modeled approximately as a surcharge applied to the soil surface. However, both the accumulated material and the undisturbed material can undergo significant deformation, and therefore disregarding the region of accumulated material leads to errors. Numerically, the process of soil cutting is difficult and inefficient to simulate using conventional methods, such as the finite element method (e.g.,

Yong 1977), discrete element method (e.g., Shmulevich et al. 2007) and material point method (e.g., Ambati et al. 2012). Hambleton (2017) describes possibilities for improving efficiency by reducing the computational complexity of existing methods.

Recently, Kashizadeh et al. (2014) and Hambleton et al. (2014) proposed a new numerical method for modelling the cutting process in sand based on incremental plastic analysis, using a concept similar to the one proposed by Mary et al. (2013). The contributions of the present work are (1) to reconcile an acknowledged contradiction in the original model, namely that the material is assumed to be incompressible even in the presence of softening (dilation) and (2) to extend the material model to allow for the possibility of hardening as well as softening. To validate the refined method to some extent, predictions are compared with preliminary experimental data.

ORIGINAL SOIL CUTTING MODEL

This section provides an overview of the original soil cutting model proposed by Kashizadeh (2018). Readers are referred to the original work for complete details of the formulation.

Deformation mechanism. Figure 1a shows the assumed deformation mechanism for the soil in front of the blade during the cutting process. All deformation occurs in a thin layer with infinitesimal thickness (i.e. slip surface), which is developed from the tip of blade to the soil surface. The angle between the slip surface and the horizontal is β. The soil above the slip surface moves as a rigid block, while the soil below is at rest. The cutting depth d keeps constant. Over the soil-blade interface, Coulomb friction is assumed, and the wall friction angle is denoted by ϕ_w. The Mohr-Coulomb yield criterion with an internal friction angle of ϕ is applied to the soil.

Based on the yield condition and equilibrium, the force P required to displace the blade can be derived and expressed as

$$P = W \frac{\tan\left(\beta + \phi\right)}{\cos\phi_w - \sin\phi_w \tan\left(\beta + \phi_w\right)} \tag{1}$$

where W is the weight of soil above the slip surface.

Numerical formulation. To simulate the cutting process, the material surface is discretized by the nodal points shown in Figure 1b. Each node represents a possible location for the slip surface. The location of the slip surface and the force P are evaluated based on the principal of minimum effort, which states that the expected deformation is the one producing the least required force. On the right-hand side of Eq. (1), the only unknown is the orientation of slip surface β. By using the grid search for optimization, i.e., minimizing the force P, the optimal orientation of the slip surface β^* and optimal force P^* within an incremental of deformation can be obtained.

After the optimal orientation of slip surface β^* is determined, the overall deformed shape is updated. Figure 1b illustrates the method of updating, where v is the incremental displacement.
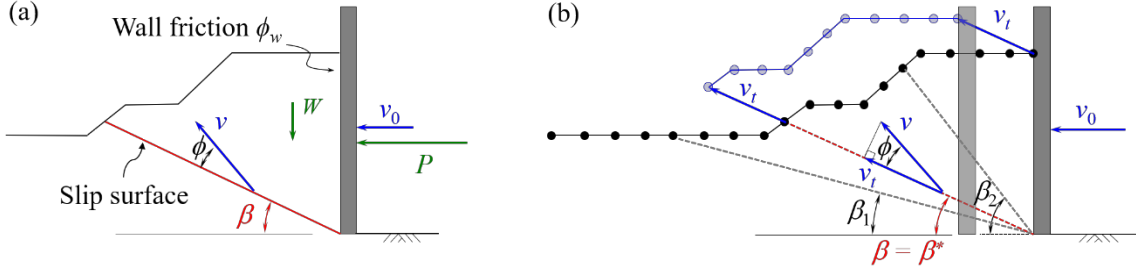
Figure 1. Original soil cutting model: (a) assumed deformation mechanism; (b) discretization, optimization and updating (Kashizadeh 2018).

In the original model, the material is assumed to be incompressible, resulting in a deformation with motion tangential to the slip surface (v_t). The magnitude of v_t is determined by the incremental displacement (velocity) of blade, denoted by v_0.

Avalanching. In sand, avalanching occurs when the inclination of the surface reaches a particular angle (the angle of repose for an infinite slope). A methodology was developed to reflect its influence, and the details are described by Kashizadeh (2018).

Material model. Figure 2a shows the material law used in the original model. The friction angle is assumed to be a function of the accumulated shearing displacement u_t, which decreases linearly from the peak friction angle ϕ_p to the residual friction angle ϕ_r at displacement u_r. The parameter u_r is here referred to as the "residual mobilization length." In the simulation, each node is assigned a unique value of u_t, and correspondingly, the friction angle can differ from node to node, reflecting the influence of softening at each shear band location.

REFINED SOIL CUTTING MODEL

The present study refines the original method in two respects. First, a shear band with finite thickness is incorporated. Second, a material law which captures the effects of hardening and softening, as well as the dilatancy and compaction within the shear band, is implemented.

Material law. In the refined model, the material law illustrated schematically in Figures 2b-c is implemented. The model neglects elastic deformation and captures the essential features of hardening and softening observed in element tests on sand (Muir Wood et al. 1994). A non-associated flow rule is used, implying that dilation angle is not equal to friction angle. Both friction angle (Figure 2b) and dilation angle (Figure 2c) are defined as a function of accumulated shearing displacement. The friction angle is assumed to increase linearly from the yield friction angle ϕ_c to the peak friction angle ϕ_p to capture hardening, and this is followed by a linear decrease of the friction angle to the residual friction angle ϕ_r to capture softening. Similarly, dilation angle is assumed to increase from ψ_c to the peak dilation angle ψ_p and then decrease to residual dilation
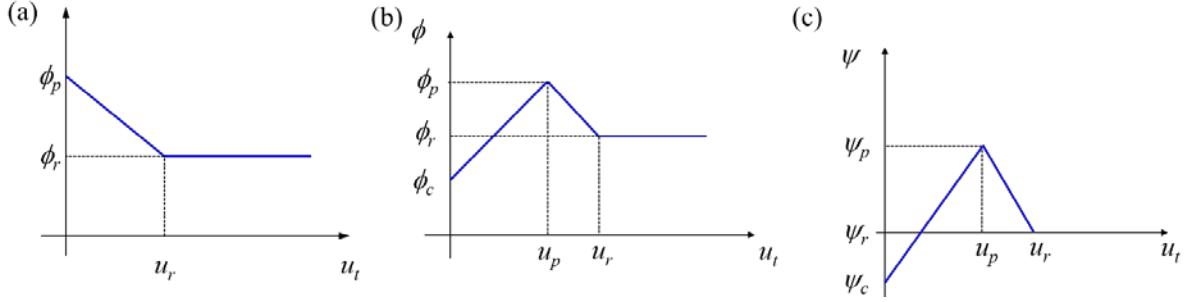
Figure 2. Variation of friction angle with accumulated displacement in (a) the original soil cutting model (Kashizadeh 2018) and (b) the refined model. (c) Variation of dilation angle with accumulated displacement in the refined model.

angle $\psi_r = 0$. The soil contracts at negative dilation angles and dilates at positive values. In the refined material law, the peak value of friction angle and dilation angle are reached simultaneously at $u_t = u_p$, and the residual values are reached at $u_t = u_r$. As in the original formulation, unique values of the accumulated shearing displacement (u_t) are assigned to each node, thus also assigning values of the friction angle and dilation angle that are updated based on the value of u_t at each step.

Incorporation of shear band thickness. Shear bands are the result of localization of deformation into thin zones of intense shearing, a phenomenon commonly observed in soils (Desrues and Viggiani 2004). In the refined model, instead of using a slip line, a shear band with finite thickness is incorporated to define the zone where the plastic deformation occurs, as illustrated in Figure 3a. The orientation of the shear band is determined through the same method used in the original numerical model (Kashizadeh 2018). A new parameter, the width of shear band (d_B), is defined in the refined model as a function of the average particle diameter d_{50}: $d_B = Nd_{50}$. The value of N normally ranges from 5 to 20 based on previous research (Mühlhaus and Vardoulakis 1987). During the cutting process, the width of the shear band is assumed to remain constant. According to the defined width d_B, the boundaries of the shear band can be located. Once the shear band is determined for one increment, the overall deformed shape and the information on the nodes within the shear band are updated based on corresponding kinematics, as shown in Figure 3c. In the refined model, volumetric changes are considered, and the soil above the lower boundary of shear band moves at an angle relative to the shear band equal to the dilation angle ψ. The magnitude of incremental displacement for the soil above the shear band is v. Within the shear band, the magnitude of incremental displacement is distributed linearly from the lower boundary to the upper boundary. At the lower boundary, the value is 0; at the upper boundary, it is v. Accordingly, the incremental shearing displacement (v_t) and volumetric displacement (v_v) are linearly distributed across the shear band. The magnitudes of these incremental displacements are fully determined by the increment of blade displacement (v_0).

Since volumetric deformation is considered, the unit weight of sand varies, and needs to be updated. At each step, the unit weight ascribed to the nodes within the shear band is assumed to be uniform, and it is calculated as $\gamma(i) = W_b/A_{new}$, where i is the nodal number within the shear

band, W_b is the weight of the band before deformation, and A_{new} is the new area of the band after deformation. As illustrated in Figure 3b, the new area of the band can be determined by the incremental shearing displacement of the blade (v_t), dilation angle (ψ), shear band width (d_B), and the area of shear band before deformation (A_0): $A_{new} = \left(v_t \tan \psi / d_B + 1 \right) A_0$. Accordingly, at each step, the unit weight on the nodes within the shear band are updated.

NUMERICAL RESULTS BASED ON REFINED MODEL

To show the performance of the refined method, two cases are studied in this section. The first is the case of a blade cutting soil with hardening-softening behavior. The second compares the cutting processes in soils with two different properties: hardening-softening and only softening.

Cutting process in hardening-softening soil. In this case, the blade cuts the soil with a depth of $d = 20$ mm. The width of the shear band is assumed to be $15d_{50}$, with $d_{50} = 0.6$ mm. The friction angle increases from $\phi_c = 20°$ to $\phi_p = 40°$ and then reduces to $\phi_r = 30°$. The dilation angle increases from $\psi_c = -5°$ to $\psi_p = 10°$ and then decreases to $\psi_r = 0$. Both the friction angle and dilation angle achieve their peak value at $u_t = u_p = 2$ mm, and reach residual values at $u_t = u_r = 4$ mm.

Figure 4 shows the progressive pattern of deformation in the cutting process predicted by the simulation. In the initial stage, the shear band develops at a shallow inclination and emerges at a location far away from the blade. It then transitions to a steeper inclination and emerges close to the blade. After this process repeats several times, the shear band remains at one position for some time corresponding to softening of the soil. After that, multiple shear bands appear at variable locations successively, leading effectively to the expression of continuous shearing. Periodically, a shear band momentarily forms far away from the blade, but it does not remain in this position long enough to accumulate appreciable deformation. As deformation accumulates, the region with the appearance of continuous shearing (the shaded region shown in Figure 4b) grows in a manner resembling the pattern detected in research on compaction bands (Papazoglou et al. 2017).

Figure 5 shows the history of the force and displacement, and the optimal orientation of the shear band (β^*) determined by optimization. To make the numerical result comparable to the
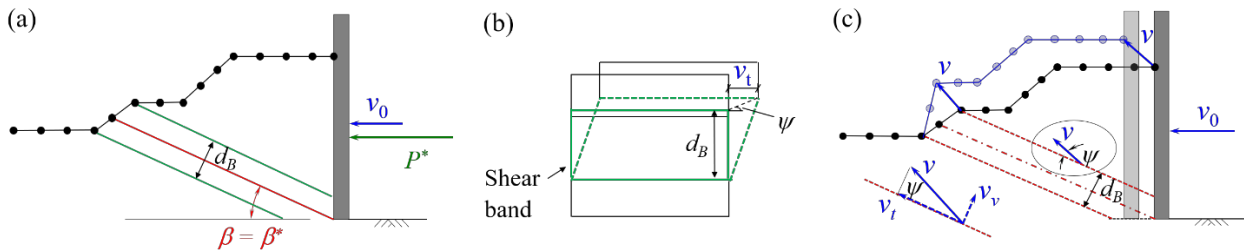

Figure 3. Refined soil cutting model: (a) incorporation of the shear band; (b) deformation of the shear band within one increment; (c) discretization, optimization and updating.
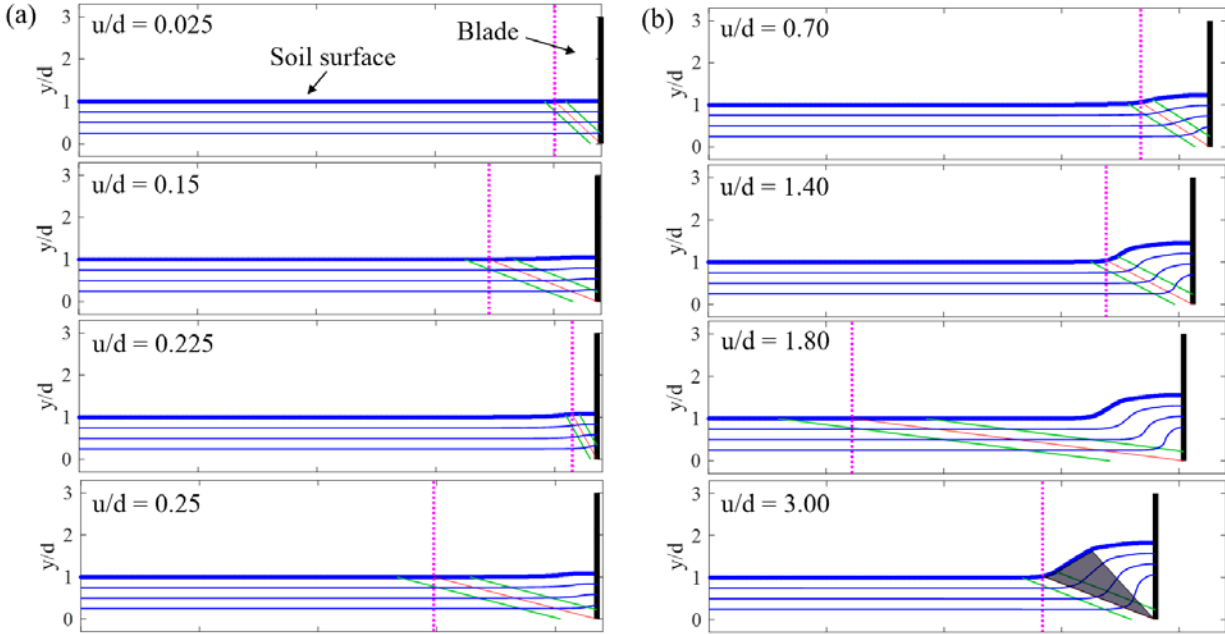
Figure 4. Progressive pattern of deformation in (a) initial stage; (b) stage of continuous shearing.
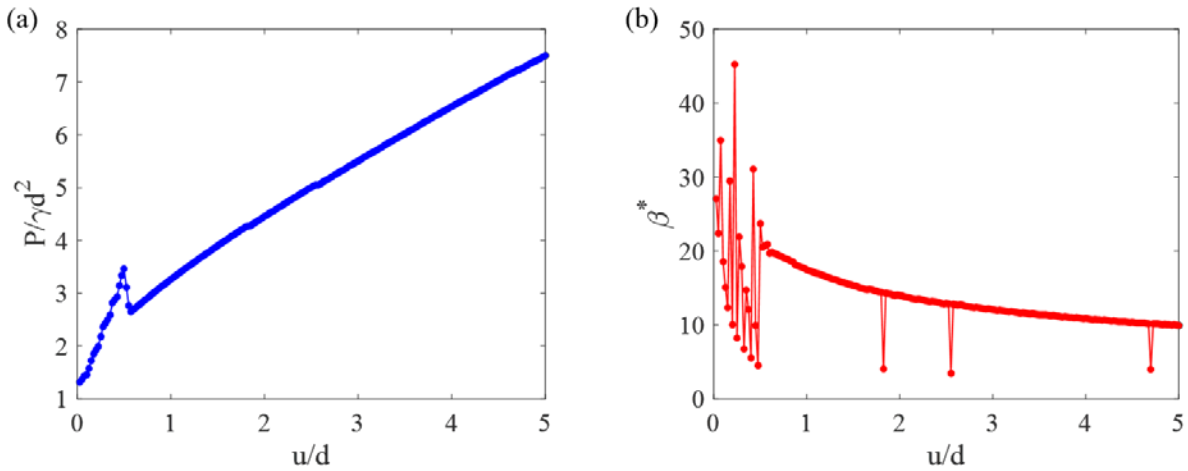

Figure 5. Numerical results of cutting in hardening-softening soil: (a) force-displacement history; (b) orientation of the shear band determined through optimization.

original studies (Kashizadeh et al. 2014, Hambleton et al. 2014, Kashizadeh 2018), the force-displacement history is normalized. It is observed that during the initial stage, which is reflected by the large cyclic variation of optimal band orientation β^*, the normalized force increases from roughly 1.3 to a peak value of roughly 3.5. After that, the normalized force decreases, corresponding to softening. Then, during the process of resembling continuous shearing, the normalized force increases gradually, followed by a subtle decrease when the shear band momentarily appears at a location far away from the blade.

Comparison of the cutting processes in soils with different properties. In this section, the soil cutting process is studied in sand with hardening-softening (HS) properties and with only softening (S) properties. The selected parameters are shown in Table 1. To make the results for these two kinds of soil properties comparable, all parameters are set to be the same except the yield friction angle ϕ_c, the dilation angle entering plasticity ψ_c, and the accumulated shearing displacement u_p required to reach the peak strength for the two cases.

Figures 6a-b show the final patterns of deformation when the displacement of the blade is $u = 5d$. For the case of sand with hardening-softening properties, multiple shear bands appear at variable locations successively, producing the impression of the continuous shear in the final pattern of deformation. For the case of soil with only softening behavior, it can be observed that shear bands appear at distinct locations, and will transition from one location to next. The normalized force-displacement history is plotted in Figure 7a. Only one peak is obtained at $u/d =1$ when the sand exhibits combined hardening and softening. However, two distinct peaks occur in the case of cutting in sand with softening only. These peaks correspond precisely to the transition of the shear band from one location to the next.

Table 1. Selected parameters for the cases of hardening-softening and softening.

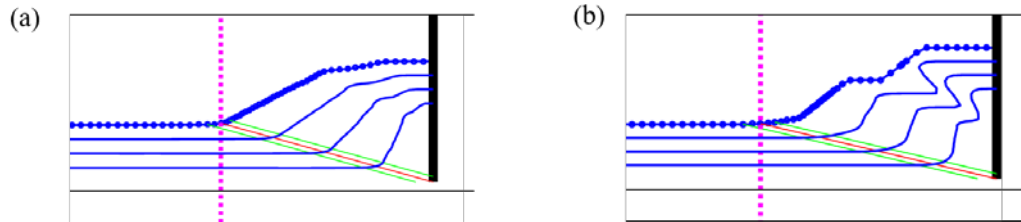|	ϕ_c (°)	ϕ_p (°)	ϕ_r (°)	ψ_c (°)	ψ_p (°)	ψ_r (°)	u_p (mm)	u_r (mm)	d(mm)	d_{50}(mm)	d_B
HS	20	35	30	-5	5	0	2	4	20	0.6	$7d_{50}$
S	35			0			0				

Figure 6. Final pattern of deformation when cutting in (a) hardening-softening soil; (b) soil with softening only.
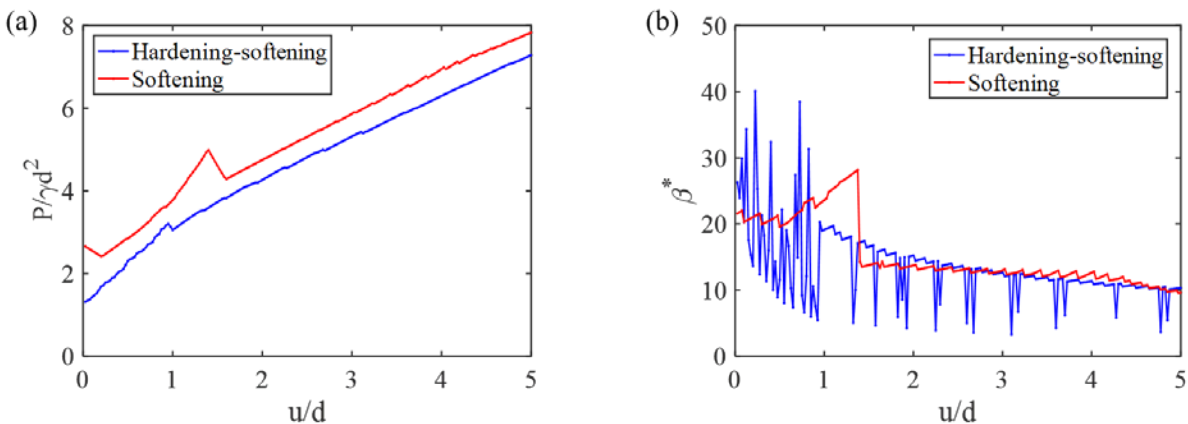

Figure 7. Comparison of (a) normalized force-displacement histories and (b) computed orientation of the shear band when cutting in hardening-softening soil and softening soil

EXPERIMENTS

Preliminary conventional (1g) laboratory tests were completed using the facilities in the SSI-SMI Laboratory at Northwestern University. These experiments were completed to obtain the full force-displacement history for comparison against the numerical predictions.

Soil preparation and experimental setup. The apparatus used in the experiment, schematically shown in Figure 8a, is comprised of a six-axis robot and a soil bed. The dimensions of the soil bed are $1500 \times 750 \times 500$ mm. In the experiments, a 17 mm thick acrylic blade with a width of 360 mm was used to model the cutting process. The experiments are quasi-2D (plain strain) given that the blade did not extend the full length (750 mm) of the soil bed, resulting in minor 3D effects at the free edge of the blade and effects of friction between the sand and the wall. However, these effects are expected to be insignificant, and the experimental technique follows well-established procedures (e.g., Hambleton and Drescher, 2008, 2009). To reduce the effect of friction between the blade and the soil bed, a Teflon sheet was stuck to the face of the blade in contact with the wall of the soil bed. The blade was first penetrated into the sand to a specified depth prior to preparing the sand sample via fluidization (Aguilar 2015). During the test, the blade was moved horizontally at a rate of 0.25 mm/s, and the displacement and horizontal force on the blade were obtained. Tests without sand were completed to measure the frictional force between the blade and the wall, and this was subtracted from the horizontal force obtained from the cutting test.

  The tests were performed on fine silica sand with a mean particle diameter of $d_{50} = 0.15$ mm. The samples were prepared by a fluidization method similar to the one describe by Aguilar (2015) to achieve a loose state. The relative density of the prepared sand sample was $D_r = 18\%$.

Results. Figure 8b shows a characteristic experimental force-displacement history compared to the prediction obtained numerically. In the computations, the parameters are assumed to be $\phi_c = 20°$, $\phi_p = \phi_r = 33°$, $\psi_c = -5°$, $\psi_p = \psi_r = 0°$, $u_p = 0.6$ mm, $d_B = 20d_{50}$ ($N = 20$), $d_{50} = 0.15$ mm. Among
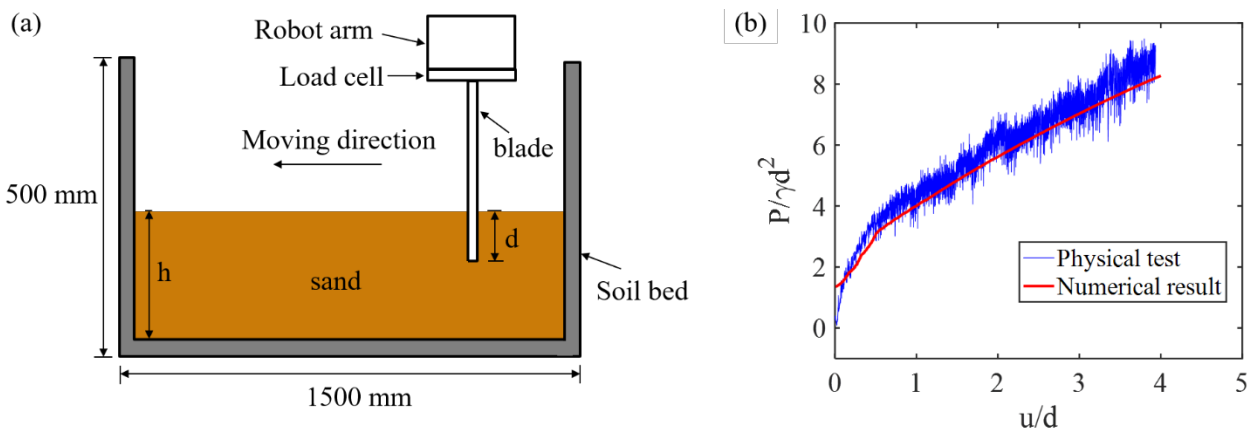
Figure 8. (a) Schematically experimental setup; (b) predicted and experimental force-displacement histories for a cutting depth of d = 25.4 mm.

these, d_{50} was the actual average particle diameter for the sand, and all other values were determined by matching the predicted force-displacement history to the measured curve. These best-fit parameters are reasonable for a loose sand, providing some level of validation for the model. However, in future work, multiple independent tests are needed for full validation.

CONCLUSIONS

This study extends the original numerical method proposed by Hambleton et al. (2014), Kashizadeh et al. (2014), and Kashizadeh (2018) in two ways: one is incorporating a shear band with finite thickness, and the other is to implement a new material law to introduce the effect of hardening and softening, as well as dilatancy and compaction within the shear band. With the modified model, it is observed in the case of hardening that shear bands successively appear to give the impression of continuous shearing in the final pattern of deformation. This is markedly different from the case of softening. With softening, the shear bands appear at distinct locations, and the transition from one location to the next is reflected in distinct peaks in the force-displacement history. In the more general case, where an initial hardening phase is followed by softening, only one peak force is obtained. The computational results are compared with the preliminary experimental data, which reveals that the predicted force-displacement history can match the results from physical tests.

Additional studies are required to further assess the validity of the refined numerical method. In particular, the proposed method relies on the strong assumption that the instantaneous mode of deformation can be represented by a single shear band of constant width throughout the entirety of the cutting process. To validate this assumption, tests examining the deformation field, e.g., using Particle Image Velocimetry (PIV), are needed. This work is presently underway in the SSI-SMI Laboratory at Northwestern University. Also, a full parametric study exploring the influence of the parameters remains to be completed.

A major practical conclusion of this work is that the cutting problem in sand, which outwardly appears complex and difficult to model by conventional numerical methods, can be simulated with a surprising level of realism using a simple and highly efficient technique. This technique can consider the full process of deformation and the influence of the accumulated soil. For full application to the earthmoving problems, future extensions of this work will consider more complex tool shapes and motions, and three-dimensional configurations.

ACKNOWLEDGEMENTS

REFERENCES

Aguilar, J. J. (2015). *Probing the Dynamics of a Simple Jumping Robot on Hard and Soft Ground*. Ph.D. Thesis, Georgia Institute of Technology, Atlanta.

Ambati, R., Pan, X., Yuan, H., and Zhang, X. (2012). Application of material point methods for cutting process simulations. *Computational Materials Science*, 57, 102–110.

Desrues, J. and Viggiani, G. (2004). Strain localization in sand: an overview of the experimental results obtained in Grenoble using stereophotogrammetry. *International Journal for Numerical and Analytical Methods in Geomechanics*, 28(4), pp. 279-321.

Godwin, R.J. and O'Dogherty, M.J. (2007). Integrated soil tillage force prediction models. *Journal of Terramechanics*, 44(1), 3–14.

Hambleton, J.P. (2017). Earthmoving through the lens of geotechnical engineering. *Proc. 6th International Young Geotechnical Engineers' Conference*, Seoul, Korea, Sept. 17-22.

Hambleton, J.P. and Drescher, A. (2008). Modeling wheel-induced rutting in soils: Indentation. *Journal of Terramechanics*, 45(6), 201-211.

Hambleton, J.P. and Drescher, A. (2009). Modeling wheel-induced rutting in soils: Rolling. *Journal of Terramechanics*, 46(2), 35-47.

Hambleton, J.P., Stanier, S.A., White, D.J., and Sloan, S.W. (2014). Modelling ploughing and cutting processes in soils. *Australian Geomechanics Journal*, 49(4), pp.147-156.

Kashizadeh, E., Hambleton, J.P., and Stanier, S.A. (2014). A numerical approach for modelling the ploughing process in sands. *Proc. 14th International Conference of the International Association for Computer Methods and Advances in Geomechanics*, Kyoto, Japan, Sept. 22-25, pp. 159-164.

Kashizadeh, E. (2018). *Theoretical and experimental analysis of the cutting process in sand*. MPhil Thesis. University of Newcastle, Australia.

Mary, B., Maillot, B., and Leroy, Y. (2013). Deterministic chaos in frictional wedges revealed by convergence analysis. *International Journal for Numerical and Analytical Methods in Geomechanics*, 37, 3036-3051.

McKyes, E. (1985). *Soil Cutting and Tillage*. Amsterdam: Elsevier.

Mühlhaus, H.B. and Vardoulakis, I. (1987). The thickness of shear bands in granular materials. *Géotechnique*, 37(3), pp. 271-283.

Papazoglou, A., Shahin, G., Marinelli, F., Dano, C., Buscarnera, G., and Viggiani, G. (2017). Localized Compaction in Tuffeau de Maastricht: Experiments and Modeling. *In: Proc. Int. Workshop on Bifurcation and Degradation in Geomaterials*. Springer, pp. 481-488.

Shmulevich, I., Asaf, Z., and Rubinstein, D. (2007). Interaction between soil and a wide cutting blade using the discrete element method. *Soil and Tillage Research*, 97, 37–50.

Wood, D. M., and Belkheir, K. (1994). Strain softening and state parameter for sand modelling. *Géotechnique*, 44(2), 335-339.

Yong, R. N. and Hanna, A. W. (1977). Finite element analysis of plane soil cutting. *Journal of Terramechanics*, 14(3), 103-125.